Faraday Discussions

Accepted Manuscript

This manuscript will be presented and discussed at a forthcoming Faraday Discussion meeting. All delegates can contribute to the discussion which will be included in the final volume.

Register now to attend! Full details of all upcoming meetings: http://rsc.li/fd-upcoming-meetings

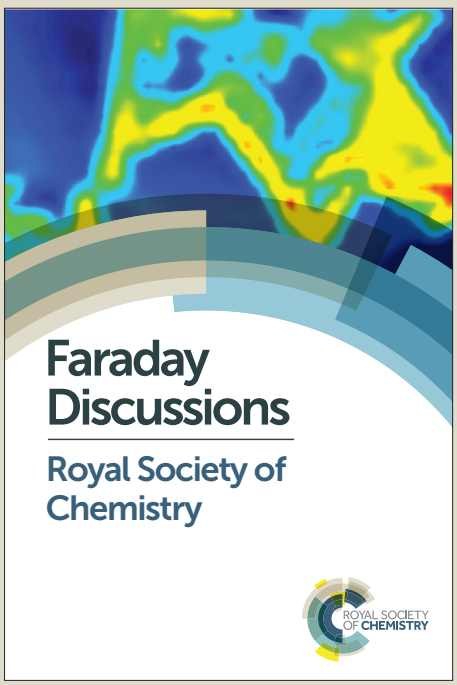

This is an *Accepted Manuscript*, which has been through the Royal Society of Chemistry peer review process and has been accepted for publication.

Accepted Manuscripts are published online shortly after acceptance, before technical editing, formatting and proof reading. Using this free service, authors can make their results available to the community, in citable form, before we publish the edited article. We will replace this *Accepted Manuscript* with the edited and formatted *Advance Article* as soon as it is available.

You can find more information about *Accepted Manuscripts* in the Information for Authors.

Please note that technical editing may introduce minor changes to the text and/or graphics, which may alter content. The journal's standard Terms & Conditions and the Ethical guidelines still apply. In no event shall the Royal Society of Chemistry be held responsible for any errors or omissions in this *Accepted Manuscript* or any consequences arising from the use of any information it contains.

ROYAL SOCIETY OF CHEMISTRY

www.rsc.org/faraday_d

CREATED USING THE RSC REPORT TEMPLATE (VER. 3.1) - SEE WWW.RSC.ORG/ELECTRONICFILES FOR DETAILS
Faraday Discussions
REVIEW www.rsc.org/xxxxxx | XXXXXXXX

Graphene as an anti-corrosion coating layer

Line Kyhl,*[a] Sune Fuglsang Nielsen[b], Antonija Grubisic Cabo[a], Andrew Cassidy[b], Jill A. Miwa[b] and Liv Hornekær[a, b]
DOI: 10.1039/b000000x [DO NOT ALTER/DELETE THIS TEXT]

Abstract

Graphene, a single layer of carbon atoms arranged in an aromatic hexagonal lattice, has recently drawn attention as a potential coating material due to its impermeability, thermodynamic stability, transparency and flexibility. Here the effectiveness of a model system; a graphene covered Pt(100) surface, for studying the anti-corrosion properties of graphene, has been evaluated. Chemical vapour deposition techniques were used to cover the single crystal surface with a complete layer of high-quality graphene and the surface was characterised after exposure to corrosive environments with scanning tunnelling microscopy and Raman spectroscopy. Graphene covered Pt samples were exposed to: i) ambient atmosphere for 6 months at room temperature and 60 °C for 75 min ii) Milli-Q water for 14 hours at room temperature and 60 °C for 75 min and iii) saltwater (0.513 M NaCl) for 75 min. at room temperature and 60 °C. STM provides atomic resolution images which show that the graphene layer and the underlying surface reconstruction on the Pt(100) surface remain intact over the majority of the surface under all conditions except exposure to saltwater when the sample is kept at 60 °C. Raman spectroscopy shows a broadening of all graphene related peaks due to hybridisation between the surface Pt d-orbitals and the graphene π-bands. This hybridisation also survives exposure to all environments except saltwater on the hot surface, with the latter leading to peaks more representative of a quasi free-standing graphene layer. A mechanism explaining the corrosive effect of hot salt water is suggested. Based on these experiments graphene is proposed to offer protection against corrosion in all environments, except saltwater on a hot surface and Raman spectroscopy is proposed as a useful method for indirectly assessing the chemical state of the Pt surface.

1 Introduction

Since the first demonstration of the remarkable electronic properties of graphene,[1] research efforts have expanded rapidly to include graphene in a range of applications, for example, ultrafast electronics,[1] sensors with single molecule sensitivity[2] or highly efficient solar cells.[3, 4] More recently, research has expanded to include graphene-based anti-corrosion coatings.[5]

An ideal material for anti-corrosion coatings for metals should possess a range of properties including being lightweight, atomically thin, impermeable, inert, wear resistant and mechanically strong. Graphene; a one-atom thin layer of carbon atoms arranged in a honeycomb lattice, satisfies all of these requirements.

Graphene transmits 97 % of irradiated light, across a broad range of the eletro-

magnetic spectrum. This can be considered an advantage in anti-corrosion coating applications where maintaining the surface optical appearance is desirable. Graphene exhibit high flexibility,[6] which can follow the curvature or roughness of the surface of an underlying substrate to a high extent. Flexibility is useful not only in coating applications but also for flexible electronics.[7, 8] Graphene is also thermodynamically stable, with stability arising from long range delocalisation of the π-electron cloud, giving rise to an extended aromatic network of C=C bonds across the entire basal plane. This chemical inertness is one of the strongest drivers justifying the use of graphene as an anti-corrosion coating. For example, graphene exposed to high pressures of superheated water, a highly corrosive cocktail, has proven more chemically stable than diamond exposed to the same conditions.[9] Graphene is able to resist reaction, breakage and penetration by superheated water when this is encapsulated in highly pressurized nano-bubbles formed at a graphene-diamond interface. The basal plane is not only chemically inert but is also impermeable. Not even He atoms can penetrate a single layer of defect-free graphene.[10]

The combination of properties described above has ignited research efforts aimed at testing the limits of graphene coatings. A range of metallic substrates has been considered and, similarly, a range of methods has been used for producing the graphene coating. Examples of studies where the graphene is shown to have a definite positive effect on the protection of metals from corrosive environments such as air, seawater, O_2 or CO, include Cu,[11-14] Pt,[15-17] Ru,[18] Ni,[12, 19, 20] Fe[21] and stainless steel 304.[22] These investigations have included both graphene grown directly on the substrate by CVD and graphene transferred after growth. Consequently graphene layers of differing quality are often compared in the literature, producing somewhat contradictory results regarding the use of "graphene" as an anti-corrosion coating. For example, reduced graphene oxide, often considered to be low-quality graphene, has been shown to protect Cu from corrosion upon exposure to a saline environment.[23] Yet, in a separate study, it has been suggested that a defected graphene coating on Cu can lead to *enhanced* corrosion of a Cu surface after long term exposure to air.[24, 25] The authors of the latter study suggested that oxides on an uncovered Cu surface block electrical contact between unreacted areas and inhibit wet corrosion. The graphene coating, however, acted as a continuous source of electrons and provided an electrical contact enabling corrosion of the entire surface. Furthermore the Cu oxide layer below the coating was stressed, since it developed with a non-uniform thickness and this led to cracks, enabling pitting and crevice corrosion. In this context it is interesting to know that graphene oxide, an insulator, has been shown to protect both Cu[26] and mild carbon steel[27] from oxidation. This may be because graphene oxide, although chemically reactive, opaque and stiff, does not conduct the electrons responsible for some of the galvanic corrosion, which has been observed to occur, in some cases, for conducting graphene coatings.

The majority of the graphene produced for coating applications is produced following chemical vapour deposition protocols on metals, since this gives large area graphene often of high quality, and with good substrate adhesion. Such graphene sheets can also be transferred to yield a graphene coating layer on other desired surfaces.[5, 28, 29] Often, however, the transferring method deteriorates the graphene quality by introducing numerous defects. Graphene coatings can be

improved by growing or transferring more layers on top of each other to seal the defected areas. Thus the possibility of using multilayer graphene as a coating is an ongoing area of study.[5, 30, 31] Such multilayer systems, however, are not suitable for all substrates and it can be difficult to accurately reproduce the same quality of graphene coating repeatedly.

The synthesis of a high quality graphene coating using conventional chemical vapour deposition (CVD) methods requires substrate temperatures > 800 °C. For more industrially relevant scenarios, recent studies have shown the synthesis of graphene coatings directly on steel and Fe surfaces to be possible.[22, 32, 33]. The high growth temperatures are, however, in many cases problematic when dealing with alloys and steels, due to phase changes and resulting reductions in mechanical properties. Research has therefore focused on finding an optimal low temperature growth procedure in order to improve the applicability for commercial applications in the coating industry. In the pursuit of a low temperature growth mechanism the use of large carbon based molecular building blocks, such as coronene or naphatelene, has proven to be advantageous.[20, 34-37] Nonetheless, controlled direct graphene growth on Fe-based substrates is difficult compared to more catalytically active transition metals, and often compromises in reproducibility and graphene quality have to be made.

DFT studies have shown that a pristine, defect-free graphene layer offers an impenetrable barrier to oxygen molecules and atoms.[38] The authors calculated a lower energy barrier for reversibly binding oxygen atoms to graphene than for the same atoms to diffuse through the graphene basal plane and reach the metal substrate below. However, the diffusion barrier through the graphene could be significantly lowered by the presence of defects, such as holes or atomic vacancies, in the graphene lattice. In line with this experimental studies demonstrates that oxygen atoms can intercalate beneath a high quality graphene layer grown on an Ir(111)[39-42] substrate. The intercalation requires slightly elevated temperatures that are thought to provide the energy required to overcome the diffusion barrier at defect sites and graphene edges allowing the oxygen atoms to diffuse beneath the graphene sheet at these areas.

Several studies highlight that the protective properties of a single graphene sheet are compromised by the presence of wrinkles, grain boundaries and atomic defects.[5, 43, 44] These areas constitute reactive sites where elements or molecules have an increased possibility of intercalating, thus reaching the substrate surface. For example, it has been shown that oxygen molecules can dissociate and bind to carbon atoms at defect sites, if those carbon atoms constitute an incomplete hexagon in the graphene lattice.[38] Once oxygen atoms are bound, the energy barrier preventing the oxygen to reach and bind to the surface below the graphene is low, and thereafter intercalation proceeds rapidly. Similarly, wrinkles in a graphene sheet stretch the carbon-carbon bonds in these regions of high curvature, thus increasing the chemical reactivity of the graphene π-bands in these areas. Breaking a C=C bond under strain is energetically more feasible than reactions on the flat basal plane. The thermal expansion coefficient of metallic substrates is larger than that of the graphene and wrinkles frequently arise during cooling of a system after the high temperature growth typical of chemical vapour deposition techniques. The challenge, therefore,

is to prevent the formation of sites facilitating the intercalation of oxidizing species since this may lead to reaction with the substrate below and thereby increase the rate of corrosion.

While reducing the defect density and/or passivating vacancy sites that act as intercalation pathways is key to increasing corrosion protection with graphene coatings,[45] it is not trivial to predict the quality of graphene required. The mechanism of protection will differ with the substrate–graphene interaction and with environment to which the system is to be exposed.[17]

The challenge, then, is to combine high resolution characterisation methods, such as scanning tunnelling microscopy with large scale, higher throughput characterisation methods, such as Raman spectroscopy. STM can provide atomic resolution of the graphene lattice and at the same time provides a topographic overview of the surface, which can be used for assessing physical changes as a function of surface reactivity. Raman spectroscopy gives data averaged over a larger area, limited in this case by the spot size of the laser on the sample. Although Raman spectroscopy from metal surfaces is usually not favourable because of the screening from the metal, graphene samples on metal substrates are well studied and several graphene-metal systems are characterised in the literature. When combined, the three graphene peaks, the D, G and 2D peaks, provide a chemical fingerprint of the graphene lattice, and their position and intensities are strongly correlated to the chemical environment of the graphene sheet. In some cases, when the graphene sheet strongly interacts with the underlying metal surface, such as graphene on Ir, the Raman signal is completely annihilated because the Raman active graphene modes hybridise too strongly with the transition metal surface d-orbitals.[46] In cases where this hybridisation is not as strong, such as graphene on Cu, Raman spectroscopy can be used to determine the quality of a graphene layer. The graphene-Pt(100) system exhibit fairly strong hybridization and Raman peaks from graphene modes, although visible, appear strongly attenuated and blue-shifted. In this article we propose to use this effect to establish the chemical state of the Pt(100) surface beneath a graphene layer. Since lifting of the Pt(100) reconstruction is associated with the formation of surface oxides, this lifting will simultaneously reduce hybridisation between the Pt surface d-orbitals and the graphene π-band. Hence, graphene becomes more free-standing and thus the Raman peaks will be red-shifted.

Previous work from our group has investigated the interaction between the Pt(100) surface and graphene with scanning tunnelling microscopy, and shown the system to be useful for investigating the anti-corrosion properties of graphene on an atomic level.[16, 17] This is facilitated by the distinct striped surface reconstruction which serves as a fingerprint of the most stable form of a clean unreacted Pt(100) surface.[47] Upon oxidation of the surface the reconstruction is lifted and the excess Pt atoms form clusters lying on top of a truncated bulk (100) arrangement of the remaining surface atoms. The surface reconstruction and its lifting can be followed by scanning tunnelling microscopy (STM), even when covered by a graphene layer.[16, 17, 48] Previous STM studies on this system has demonstrated that graphene acts as an effective anti-corrosion coating against O_2 and H_2S, while CO was shown to intercalate at the graphene-Pt(100) interface for pressures above 10^{-6} mbar.[16, 17] Here we test the stability of the graphene-Pt(100) system towards air, water and saltwater

while keeping the sample at either room temperature or at 60 °C. For the first time, we also relate the lifting of the Pt(100) surface reconstruction, following the oxidation of the Pt surface, to changes in peak positions and intensities in Raman spectroscopy. The graphene coating was observed to be effective in protecting the Pt surface from reactions with air and water, while it was observed to fail under salt water at 60 °C, where a lifting of the Pt(100) surface reconstruction was observed by STM and via a shift in Raman peak intensity and position.

2 Experimental Methods

Graphene samples were prepared in an ultra-high vacuum chamber with a base pressure of $5x10^{-10}$ mbar. Pt(100) single crystal samples were cleaned by several cycles of argon sputtering followed by flash annealing to 900 °C. For graphene growth the sample was maintained at 700 °C and exposed to ethylene gas at a partial pressure of $5x10^{-7}$ mbar for 40 min. The sample was subsequently annealed to 800 °C in UHV for 5 min. Low-energy electron diffraction (LEED) (Omicron Nanotechnology GmbH) was performed to check the quality of the prepared graphene. Scanning tunnelling microscopy was performed in air using an Aarhus-type STM[49] with a cut Pt/Ir tip. The distances measured by STM are accurate to within 10% of the quoted values. These uncertainties are due to piezo creep and/or thermal drift.

Raman spectra were obtained using a Renishaw Invia Reflex Raman Spectroscopy System. All spectra were obtained using a 457 nm Ar-ion laser with a 10 s acquisition time and 50 accumulations per spectrum through a 100x objective. Spectra were taken at several points for each sample and the spectra shown here are representative thereof.

To test the stability of graphene as an anti-corrosion coating, the samples were exposed to: (i) ambient conditions (22 ˚C in air), (ii) ultra-pure water (type 1, Milli-Q grade), and (iii) a seawater analogue prepared by dissolving pure NaCl in Milli-Q water (0.513 M NaCl). Where samples were heated to 60 ˚C a hot plate was used. A k-type thermocouple mounted on the back of a dummy sample of the same thickness, also placed on the hot plate, was used to measure the temperature.

For short term exposures to solutions, *i.e* < 75 min., the solutions were continuously added to maintain a full surface coverage. For longer term exposures to Milli-Q water, *i.e.*14 hour, a humidity chamber was built and used to reduce the rate of water evaporation during the experiment.

3 Results

A graphene layer was grown on a clean Pt(100) surface following the recipe described in the Experimental section. This pristine graphene-Pt system was characterised and the results are shown in fig. 1. Fig. 1a shows a low-energy electron diffraction (LEED) pattern collected immediately after growth under ultra-high vacuum conditions. Fig. 1b shows a representative scanning tunnelling microscope image and fig. 1c a Raman spectrum, both collected under ambient conditions. In the LEED pattern in fig. 1a both the striped pattern resulting from Hex-R0.7° reconstruction of the Pt(100) surface and a ring arising from the graphene

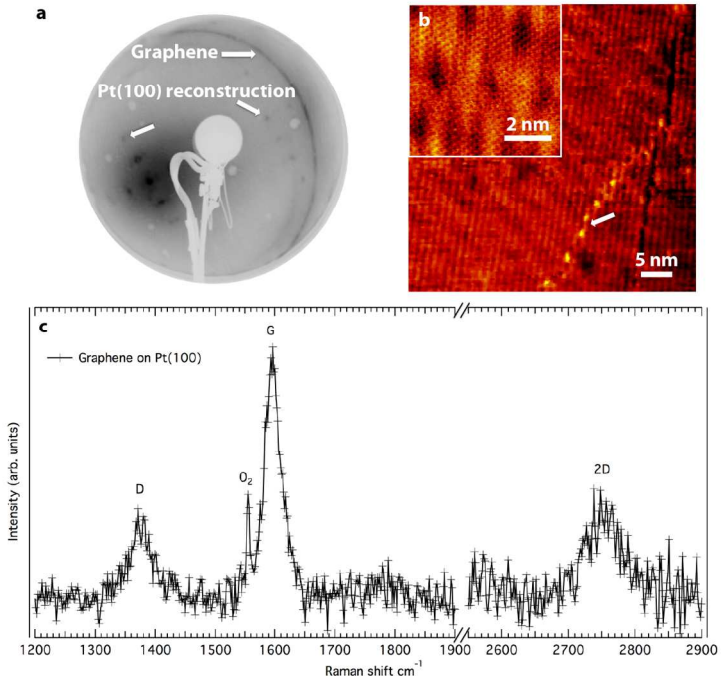

Fig. 1.: Characterization of a pristine graphene-Pt(100) sample. a) LEED pattern (E_0 = 75 eV) for a graphene covered Pt(100) surface recorded under UHV. Points representing the striped Hex-R0.7° reconstruction are marked with arrows. The dark circle representing graphene domains is also marked with an arrow. b) An STM image recorded under ambient conditions showing the Pt(100) surface reconstruction depicted as lines running almost vertically. A graphene grain boundary is marked by an arrow. I_t = 0.640 nA, V_t = 275.3 mV. The inset shows an atomic resolution image of the graphene covering the reconstructed Pt surface. I_t = 1.080 nA, V_t = 59.2 mV. c) A Raman spectrum of the pristine graphene-Pt(100) sample. The spectrum shows three peaks relevant for the graphene: D, G and 2D, and one peak originating from O_2 present in the air. The peak positions are 1375 cm^{-1}, 1596 cm^{-1}, 2753 cm^{-1} and 1556 cm^{-1} respectively.

layer are visible. The weak interaction between graphene and the reconstructed Pt(100) surface does not drive a preferred angular orientation between different graphene domains, resulting in the circular diffraction pattern visible in LEED experiments.[50] The STM image in fig. 1b also depicts the Pt surface reconstruction and the graphene layer, the later visible with atomic resolution in the inset image. The Pt surface reconstruction appears as row of atoms running from top to bottom in the larger scale image. This is also visible to some extent in the inset. The visibility of the reconstruction under ambient conditions demonstrates that the graphene layer protects the underlying Pt surface from immediate reactions with the ambient environment. Raman spectroscopy, taken of the same sample under the same conditions reveals four distinct peaks, fig. 1c. Three of these peaks are related to the

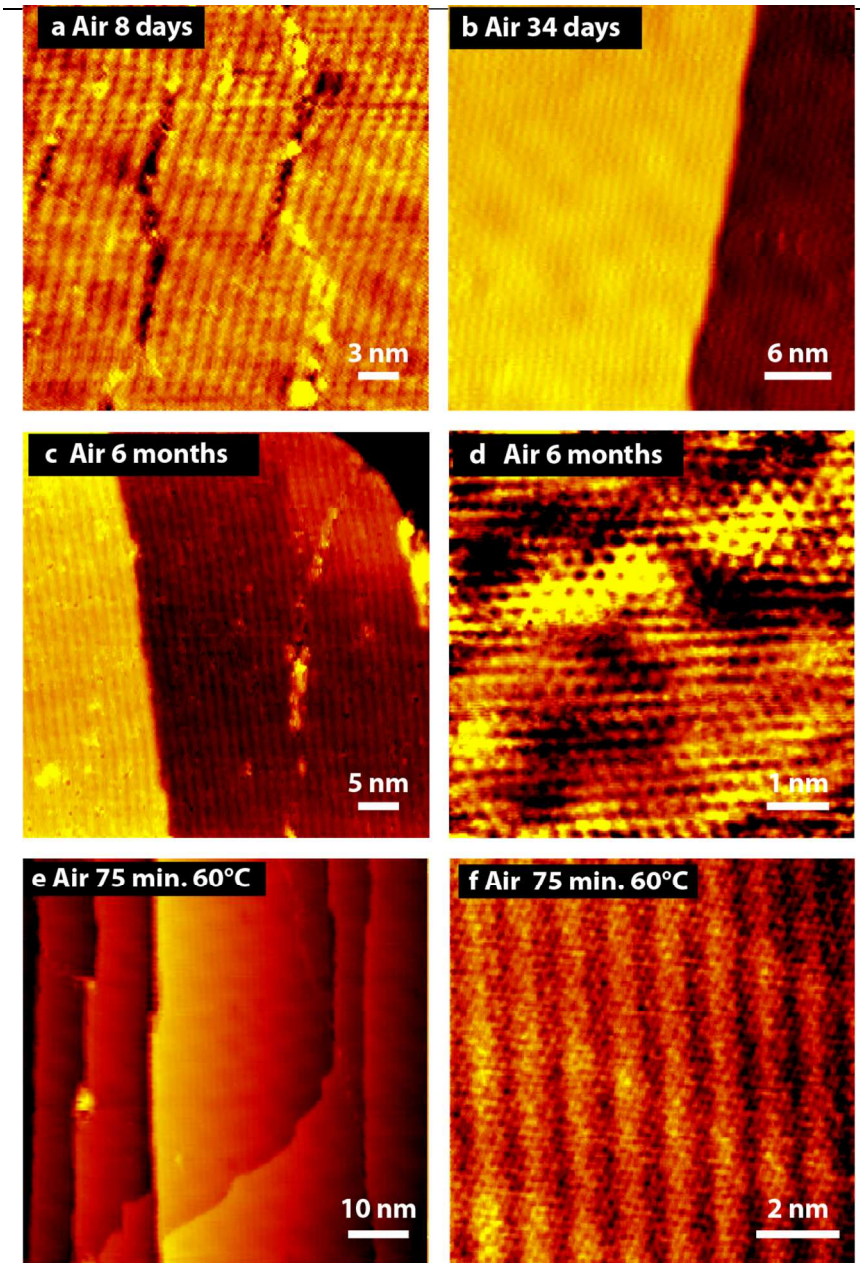

Fig. 2: STM images of graphene-Pt(100) following air exposure at room temperature a)-d) and at 60 °C e)-f). a) After 8 days I_t = 0.960 nA, V_t = 4.0 mV b) after 34 days I_t = 0.350 nA, V_t = 55.8 mV c-d) after 6 months. c) I_t = -0.570 nA, V_t = - 630.0, d) shows an atomic resolution image in an area of lifted reconstruction. I_t = -1.080 nA, V_t = - 374.1 mV. e) After 75 min. air exposure at 60 °C showing intact reconstruction running as vertical lines on the Pt terraces. I_t = 0.280 nA, V_t = 131.8 mV. f) Atomic resolution of the graphene coating covering the Pt(100) reconstruction. I_t = 0.750 nA, V_t = 24.4 mV.

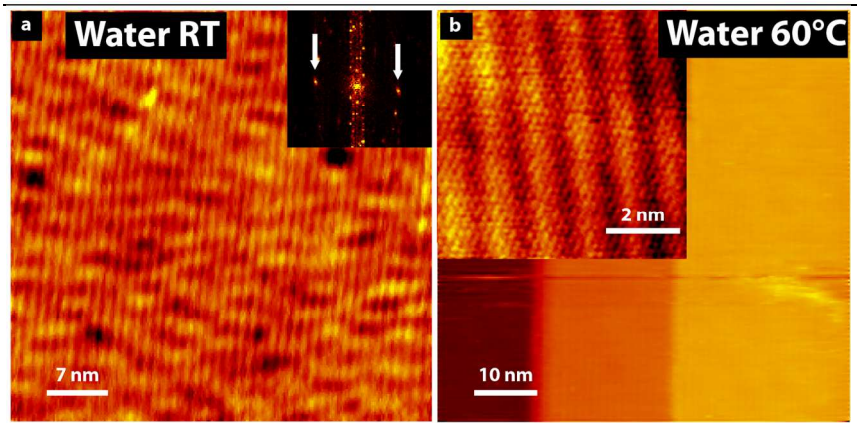

Fig. 3.: STM images of graphene-Pt(100) exposed to water for a) 14 hours at room temperature. I_t = 0.260 nA, V_t = 18.6 mV. Noise has been filtered from this image to reveal the Pt(100) reconstruction. A fast fourier transform of the image is depicted in the inset (upper right corner) with arrows marking the points corresponding to the reconstruction. b) 75 min. at 60 °C showing the intact reconstruction running as vertical lines on the Pt terraces in the image. I_t = -0.260 nA, V_t = -1277.1 mV. Inset shows atomic resolution of the graphene coating covering the intact Pt reconstruction. I_t = 0.680 nA, V_t = 220.9 mV.

graphene layer: i) a low intensity D peak at 1376 cm^{-1}; ii) a G peak at 1596 cm^{-1} and iii) a 2D peak at 2753 cm^{-1}. The last peak at 1556 cm^{-1} can be attributed to O_2 from the air. These peaks have been assigned on the basis of calculations performed on graphene on a Pt substrate.[46] By fitting the peaks with Lorentzian functions, a D/G intensity ratio of 0.32 was measured. Using the empirical relation $L_D^2(nm^2) = (1.8 \pm 0.5) \times 10^{-9} \lambda_L^4 (I_D/I_G)^{-1}$, where L_D is the distance between defects, λ_L is the laser wavelength in nm, and I_D and I_G are the peak intensities of the D and G peaks respectively, yields $L_D = 16\,\mathrm{nm}$.[51] The equation is valid assuming a defect distance larger than 10 nm, which is supported by analysis of the STM images.

Following the preparation and characterisation of the pristine graphene-Pt(100) system, stability tests were performed in order to test the limits of graphene as an anti-corrosion protective barrier. Experiments may be divided into three categories testing against: i) Air: A 6 month study at room temperature and a 75 min. test at 60 °C, ii) water: a 14-hour test at room temperature and a 75 min. test at 60 °C, iii) saltwater: A 75 min. test at room temperature and a 75-min. test at 60 °C. Scanning tunnelling microscopy was performed for all experiments (figs. 2, 3 and 4) and Raman spectra were obtained from samples exposed to 75 min. tests (fig. 5). The coating was deemed successful if the STM images revealed the survival of the Pt(100) surface reconstruction over most of the surface and the Raman shift for graphene peaks did not move to lower wavenumbers, relative to the shifts measured for the pristine graphene-Pt(100) system. As will be shown below, the graphene coating was successful in all cases aside from the 75 min. 60 °C saltwater test.

Fig. 2 shows STM results from the stability test against air. A pristine graphene-Pt(100) system was left in ambient air for a period of 6 months and periodically characterised. Fig. 2 includes representative images after a) 8 days, b) 34 days and c)

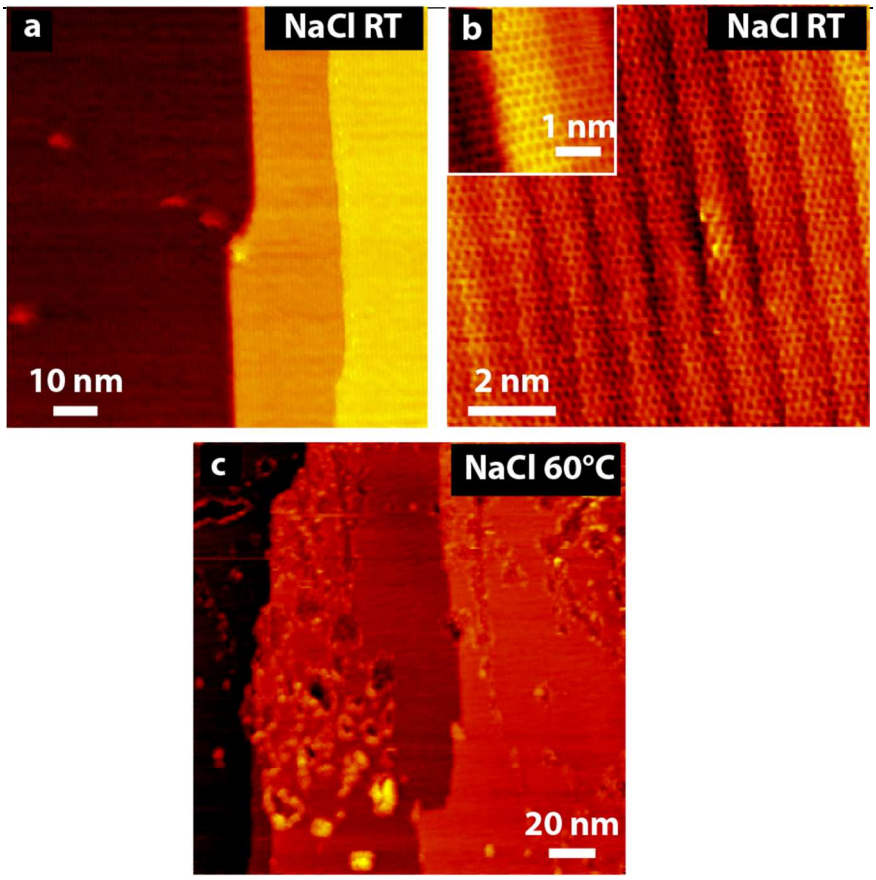

Fig. 4.: a-c) STM results following 75 min. exposure of graphene-Pt(100) to saltwater (0.513 M) a)-b) at room temperature, a) I_t = -0.260 nA, V_t = -611.3 mV. b) Atomic resolution of the graphene coating covering the intact Pt reconstruction. I_t = -0.970 nA, V_t = -2.7 mV. The inset shows a zoom on the graphene coating depicting the hexagonal pattern of the graphene. I_t = -0.950 nA, V_t = -2.7 mV. c) At 60 °C. I_t = 0.470 nA, V_t = 1250.0 mV. The image shows a roughening of the surface consisten with what is expected from a lifted Pt reconstruction.

and d) 6 months. In fig. 2a-c it is evident that the reconstruction of the Pt(100) surface, represented in the images as vertical lines running from top to bottom, remains predominantly intact. In figs. 2b and 2c the bright and dark areas represent two different terraces, separated by a step edge running from top to bottom, on the Pt surface. In fig. 2c there are some areas were the Pt reconstruction has begun to lift, represented by the bright protrusions in the image. An atomically resolved image of an area with lifted reconstruction is shown in fig. 2d. From this image it is evident that the graphene carbon lattice remains intact despite the lifting of the reconstruction. The larger light and dark areas of contrast in this image reflect the topography of the underlying Pt surface. The Pt(100) surface increases in roughness in response to the lifting of the reconstruction.[16] In a separate experiment a graphene-Pt(100) sample was heated in ambient air conditions to 60 °C. The STM results are shown in figs. 2e&f. In fig. 2e multiple flat terraces on the graphene

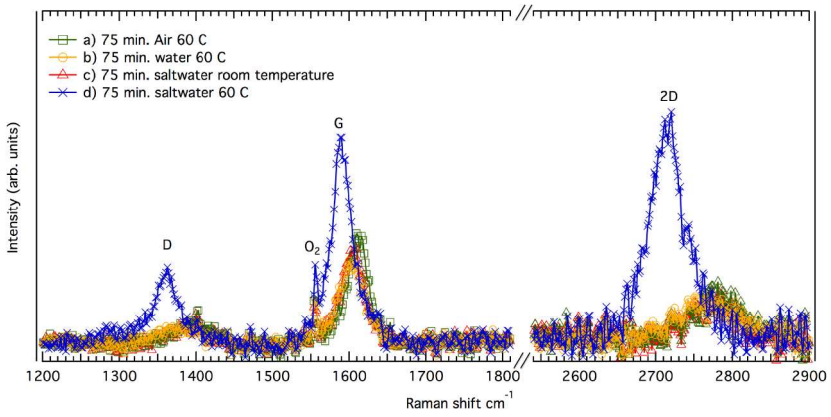

Fig. 5.: Raman spectra corresponding to samples exposed to: a) 75 min., air, 60 °C, b) 75 min., water, 60 °C, c) 75 min., saltwater, room temperature and d) 75 min. saltwater 60 °C. Plotted with a a) green square, b) yellow circle, c) red triangle and d) blue cross. Spectra a-c have similar peak shapes and positions while in spectrum d the peaks have shifted and increased in intensity.

covered Pt(100) surface are shown. The reconstruction is observed to be intact, visible as lines running vertically on the terraces. In fig. 2f atomic resolution of the graphene covering the intact reconstruction is shown.

The stability of the graphene coating against water was also tested and STM results are presented in fig. 3. Fig. 3a shows a representative STM image following exposure of a pristine graphene-Pt(100) sample to Milli-Q water for 14 hours at room temperature. The image has been filtered to remove background noise. A spatial fast fourier transform (FFT) of the (unfiltered) image is included in the inset with white arrows pointing out the spots arising from the intact reconstruction. The intact reconstruction confirms that the graphene protects the Pt(100) surface from reaction with water at room temperature for at least 14 hours. In a separate experiment, a pristine graphene-Pt(100) sample was exposed to Milli-Q water at 60 °C, and a representative STM image of the resulting surface is included in fig. 3b. The reconstruction remains visible on the surface, indicating efficient coating performance under these conditions.

Finally the stability of the graphene coating was tested against saltwater. A saltwater solution (0.513 M) was prepared as an analogue to the Northsea (0.56 M). Two 75 min experiments were performed, figs. 4a&b with the sample at room temperature and fig. 4c with the sample at 60 °C. In figs. 4a&b the reconstruction, running as vertical lines in the images, remains intact. Fig. 4b shows atomic resolution of the graphene layer with the intact reconstruction visible beneath. The inset in fig. 4b shows a close-up of the graphene honeycomb lattice. The images show that the surface remains unperturbed and the graphene coating protects the Pt surface.

Fig. 4c shows a representative STM image following the second experiment, where the sample was heated to 60 °C while exposed to the saltwater solution. The surface

roughness has increased, this is especially visible in the left side of the image. This roughness represents the lifting of the Pt(100) surface reconstruction below the graphene layer, suggesting that the graphene coating has failed to protect the Pt surface from reaction with hot saltwater.

Fig 5 shows Raman spectra collected from samples exposed to a) (green squares) 75 min in air at 60 °C b) (yellow circles) 75 min in water at 60 °C c) (red triangles) 75 min in saltwater at room temperature and d) (blue crosses) 75 min in saltwater at 60 °C. There are four peaks visible in each Raman spectrum and they are labelled as they were for the pristine graphene-Pt(100) system in fig. 1c; three peaks corresponding to the graphene layer (D, G and 2D peaks) and an O_2 peak from oxygen molecules present in the air. Peak positions and intensities were determined by fitting with Lorentzian functions. The Raman spectra can be divided into two distinct groups, the first group shows peak positions similar to the pristine graphene-Pt(100) system shown in fig. 1c. These data relate to the 75 min. ambient saltwater test, the 75 min. 60 °C air test and the 75 min. 60 °C water test. I_D/I_G ratios for this group yield an average value of 0.20 ± 0.016, giving a defect distance, $L_D = 20\,\text{nm}$, indicating lower defect density than that for the pristine graphene-Pt(100) presented in fig. 1c (where $L_D = 16\,\text{nm}$). This indicates that the defect density may vary between different growth cycles and/or may not be homogeneous across the graphene layer.

The Raman spectrum relating to the 75 min. 60 °C saltwater test is obviously different from the spectra in group one; peak positions are red-shifted and the relative as well as the absolute intensities of the individual peaks have changed. The D peak has shifted to 1361 cm^{-1}, the G peak to 1590 cm^{-1} and the 2D peak to 2715 cm^{-1}. The I_D/I_G ratio has increased to 1.1 corresponding to an estimated defect distance, $L_D = 8\,\text{nm}$. It was not possible to obtain STM data with sufficient resolution to confirm this L_D, which is below the threshold that would allow use of the empirical relation between I_D/I_G and L_D.[51]

4 Discussion

In this work it has been demonstrated that graphene protects the surface reconstruction on the Pt(100) surface from reactions with oxidising species under ambient conditions for up to 6 months, from reactions with water for up to 14 hours, and from reactions with air and water at 60 °C for at least 75 min. However, during the long term stability test in air (fig. 2) the Pt surface reconstruction was observed to be lifted in some small, confined areas on the surface after 6-months (fig. 2d). It is expected that these areas are related to small scale defects such as grain boundaries which were already present on the pristine graphene-Pt(100) system following the initial graphene growth. As discussed in the introduction, it is anticipated that it is only at these sites that oxidising species can penetrate the graphene coating layer. After this initial penetration, the lifting of the surface reconstruction is diffusion limited as impurities intercalate between the graphene sheet and the Pt surface. This was illustrated by the atomic scale lattice presented over the area of lifted reconstruction in fig. 2d. The graphene lattice remains intact despite the lifting of the underlying reconstruction. Since the perfect graphene layer should be impenetrable for the oxidising species and since no etching of the

graphene at this site is observed, the observations indicate that the oxidising species arrived at this site by diffusing beneath the graphene layer after intercalating at some defect site outside of the imaged area. Interestingly, the diffusion process does not seem to be very efficient in this case, since the reconstruction was only observed to be lifted in a few small, confined areas on the surface.

While STM only give local information on small areas of the surface, Raman spectroscopy is a global technique frequently used to assess the quality of a graphene layer on a multitude of substrates. Typically the ratio between the intensities of the 2D/G peaks is used to assess the number of layers of graphene which have been produced and the quality of the graphene layer can be assessed by the ratio between the intensities of the D/G peaks. The Raman spectrum in fig. 1c, representing a pristine graphene-Pt(100) system, shows relatively broad peaks, which are low in intensity compared to the background noise level. This is not a reflection, however, on the graphene quality, but instead is a by-product of the presence of the underlying Pt substrate. Raman signals from metals are weak because of the metal-screening effect. Even so graphene samples on very weakly interacting metallic substrates, like Cu, produce well-resolved Raman spectra. In the graphene-Pt(100) system, however, hybridization of the metallic Pt d-states with the graphene π-orbitals leads to a large reduction in Raman intensity and a blue-shift in graphene-related peaks.[46] Calculations can be used to compare the change in the 2D peak wavenumber and the level of hybridization.[46] Thus, for quasi free-standing graphene, where overlap between the Pt d-states and the graphene π-orbitals is reduced, the 2D peak moves to lower wavenumbers and becomes more narrow. In the Raman spectrum in fig. 1c, which represents pristine graphene, and the Raman spectra in fig. 5a-c corresponding to unreacted graphene-Pt(100) systems, the 2D peak occurs at a higher wavenumber, is broad and is reduced in intensity due to hybridisation effects. The D and G peaks in these Raman spectra are similarly blue-shifted and reduced in intensity. Once the Pt substrate has been oxidised following exposure to saltwater at 60 °C, the D, 2D and G peaks are red-shifted, and gain in absolute intensity. The intensity gain is probably caused both by an increased separation between the metal surface and the graphene sheet, reducing the metal-screening effect and by a reduction in hybridisation between the Pt surface d-orbitals and the graphene π-band.[46] The observed shift in peak position is also expected from this change in hybridisation. However a change in graphene strain, caused by the formation of a rough Pt oxide layer on the surface, has also been suggested to lead to a shift in Raman peak positions.[52] Hence the Raman data can be used to indirectly assess the chemical state of the Pt substrate. That the Raman spectrum recorded from high temperature, salt-water exposed graphene-Pt(100) more closely resembles free-standing graphene concurs with the conclusion from STM data, namely that the reconstruction has lifted. This red-shift in the Raman-active graphene modes was accompanied by both an absolute and relative change in peak intensities, fig. 5c. An attempt was made to extract the defect density from the new I_D/I_G ratios, but the result was inconclusive. Since the intensities of the Raman peaks are influenced by the hybridization with the surface, it is unclear if the change in I_D/I_G ratio resulted from an increase in defect density or relates to the change in hybridisation of the graphene π-band.

The combination of heat and saltwater was observed to lead to large scale coating

breakdown and reaction with the Pt surface. Previous DFT calculations have examined the edge state of graphene islands on a Pt surface and concluded that in the presence of OH^- groups an open-edge configuration is favoured.[17] This open-edge configuration sees the OH- groups react with and separate edge-C atoms on the graphene sheet from the underlying Pt surface atoms. The resulting open edge configuration allows atoms and molecules to intercalate beneath the graphene layer and facilitates reaction with the Pt surface. A temperature of 60 °C is not sufficient to break the bond between graphene C-edge atoms and the underlying Pt atoms, without involving edge-reactions with external species. The Na^+ and Cl^- ions in the saltwater may extend the lifetime of transient OH^- and H+ groups in solution when compared to the pure water solution. These charged species may increase the possibility for reactions involving edge-C atoms at defects and grain boundaries in the graphene sheet. Since no coating breakdown is observed for room temperature saltwater, we speculate that the activation energy barrier for these reactions makes them inefficient at room temperature.

5 Conclusion

A continuous single layer of graphene was prepared on a single crystal Pt(100) surface. Raman spectroscopy in combination with STM was used to detect the conditions under which this coating was compromised. The graphene layer successfully protected the Pt surface, as determined by the survival of the Pt(100) surface reconstruction, from oxidising in air for up to 6 months, water for up to 14 hours and NaCl solution for up to 75 min. at room temperature. When the sample was exposed to salt water at 60 ˚C, the Pt(100) surface reconstruction was observed to lift. STM imaging provided high resolution data, and this was combined with Raman spectroscopy to study the changes to the surface structure and chemistry. STM images revealed that the graphene carbon lattice can remain intact, even if the underlying Pt surface has been oxidised. This suggests that oxidising species do not etch intact areas on the graphene basal plane, but instead diffuse beneath the graphene layer having first intercalated at defects in the graphene lattice. Such defects probably originate during the original growth procedure, predominantly at grain boundaries. It is noteworthy, however, that the Pt surface was not oxidised in air for an extended period of time. Even after 6 months of exposure the areas where the reconstruction was lifted were few and small in size. An uncovered Pt(100) surface oxidises in seconds following exposure to air, so the graphene layer offers significant protection.

Atomic resolution in STM experiments was not achieved on samples exposed to a combination of heat and salt water. This means that it was not possible to discern whether or not the graphene basal plane was compromised under these conditions. Certainly the underlying Pt surface changed both structurally as determined from STM images, and chemically as determined from Raman spectroscopy. It is proposed that these changes represent a lifting of the Pt(100) surface reconstruction, heralding the oxidation of the Pt metal surface.

References

[a] *Interdisciplinary Nanoscience Center, Aarhus University, Gustav Wieds Vej 14, 8000 Aarhus C, Denmark. Tel: +45 871 55695; Email: line1@inano.au.dk.*
[b] *Department of Physics and Astronomy, Aarhus University, Ny Munkegade 120, 8000 Aarhus C, Denmark. Tel: +45 871 56336; E-mail: liv@phys.au.dk*

1. K. S. Novoselov, A. K. Geim, S. V. Morozov, D. Jiang, Y. Zhang, S. V. Dubonos, I. V. Grigorieva and A. A. Firsov, *Science*, 2004, **306**, 666-669.
2. T. Kuila, S. Bose, P. Khanra, A. K. Mishra, N. H. Kim and J. H. Lee, *Biosensors & Bioelectronics*, 2011, **26**, 4637-4648.
3. Y. Z. Zhang, T. Liu, B. Meng, X. H. Li, G. Z. Liang, X. N. Hu and Q. J. Wang, *Nature Communications*, 2013, **4**.
4. Y. L. Chen, X. B. Feng and D. D. Hou, *Acta Physica Sinica*, 2013, **62**.
5. D. Prasai, J. C. Tuberquia, R. R. Harl, G. K. Jennings and K. I. Bolotin, *Acs Nano*, 2012, **6**, 1102-1108.
6. C. Gomez-Navarro, M. Burghard and K. Kern, *Nano Letters*, 2008, **8**, 2045-2049.
7. S. K. Lee, H. Y. Jang, S. Jang, E. Choi, B. H. Hong, J. Lee, S. Park and J. H. Ahn, *Nano Letters*, 2012, **12**, 3472-3476.
8. C. Sire, F. Ardiaca, S. Lepilliet, J. W. T. Seo, M. C. Hersam, G. Darnbrine, H. Happy and V. Derycke, *Nano Letters*, 2012, **12**, 1184-1188.
9. C. Lim, A. Sorkin, Q. L. Bao, A. Li, K. Zhang, M. Nesladek and K. P. Loh, *Nature Communications*, 2013, **4**.
10. R. R. Nair, H. A. Wu, P. N. Jayaram, I. V. Grigorieva and A. K. Geim, *Science*, 2012, **335**, 442-444.
11. S. S. Chen, L. Brown, M. Levendorf, W. W. Cai, S. Y. Ju, J. Edgeworth, X. S. Li, C. W. Magnuson, A. Velamakanni, R. D. Piner, J. Y. Kang, J. Park and R. S. Ruoff, *Acs Nano*, 2011, **5**, 1321-1327.
12. N. T. Kirkland, T. Schiller, N. Medhekar and N. Birbilis, *Corrosion Science*, 2012, **56**, 1-4.
13. J. H. Huh, S. H. Kim, J. H. Chu, S. Y. Kim, J. H. Kim and S. Y. Kwon, *Nanoscale*, 2014, **6**, 4379-4386.
14. Y. Q. Liang, L. L. Yu, Z. D. Cui, S. L. Zhu, Z. Y. Li and X. J. Yang, *Science of Advanced Materials*, 2014, **6**, 545-549.
15. R. T. Mu, Q. Fu, L. Jin, L. Yu, G. Z. Fang, D. L. Tan and X. H. Bao, *Angewandte Chemie-International Edition*, 2012, **51**, 4856-4859.
16. L. Nilsson, M. Andersen, R. Balog, E. Laegsgaard, P. Hofmann, F. Besenbacher, B. Hammer, I. Stensgaard and L. Hornekaer, *Acs Nano*, 2012, **6**, 10258-10266.
17. L. Nilsson, M. Andersen, B. Hammer, I. Stensgaard and L. Hornekaer, *Journal of Physical Chemistry Letters*, 2013, **4**, 3770-3774.
18. B. Borca, F. Calleja, J. J. Hinarejos, A. L. V. de Parga and R. Miranda, *Journal of Physics-Condensed Matter*, 2009, **21**.
19. Y. S. Dedkov, M. Fonin and C. Laubschat, *Applied Physics Letters*, 2008, **92**.
20. U. Mogera, N. Kurra, D. Radhakrishnan, C. Narayana and G. U. Kulkarni, *Carbon*, 2014, **78**, 384-391.
21. Y. S. Dedkov, M. Fonin, U. Rudiger and C. Laubschat, *Applied Physics Letters*, 2008, **93**.
22. R. John, A. Ashokreddy, C. Vijayan and T. Pradeep, *Nanotechnology*, 2011, **22**.
23. S. C. Sahu, A. K. Samantara, M. Seth, S. Parwaiz, B. P. Singh, P. C. Rath and B. K. Jena, *Electrochemistry Communications*, 2013, **32**, 22-26.

24. M. Schriver, W. Regan, W. J. Gannett, A. M. Zaniewski, M. F. Crommie and A. Zettl, *Acs Nano*, 2013, **7**, 5763-5768.
25. F. Zhou, Z. T. Li, G. J. Shenoy, L. Li and H. T. Liu, *Acs Nano*, 2013, **7**, 6939-6947.
26. K. Krishnamoorthy, A. Ramadoss and S. J. Kim, *Science of Advanced Materials*, 2013, **5**, 406-410.
27. J. H. Park and J. M. Park, *Surface & Coatings Technology*, 2014, **254**, 167-174.
28. G. Libo, N. Guang-Xin, L. Yanpeng, L. Bo, A. H. Castro Neto and L. Kian Ping, *Nature*, 2014, **505**, 190-194.
29. J. Lee, Y. Kim, H. J. Shin, C. Lee, D. Lee, S. Lee, C. Y. Moon, S. C. Lee, S. J. Kim, J. H. Ji, H. S. Yoon and S. C. Jun, *Acs Applied Materials & Interfaces*, 2014, **6**, 12588-12593.
30. V. Migkovic-Stankovic, I. Jevremovic, I. Jung and K. Rhee, *Carbon*, 2014, **75**, 335-344.
31. Y. Su, V. G. Kravets, S. L. Wong, J. Waters, A. K. Geim and R. R. Nair, *Nature Communications*, 2014, **5**.
32. A. Hyosub, L. Won-Jun and J. Jongwan, *Current Applied Physics*, 2011, **11**, S81-S85.
33. R. S. Edwards and K. S. Coleman, *Accounts of Chemical Research*, 2013, **46**, 23-30.
34. W. Tianru, D. Gugiao, S. Honglie, W. Haomin, S. Lei, Z. Yun, J. Da and X. Xiaoming, *Nanoscale*, 2013, **5**, 5456-5461.
35. Z. C. Li, P. Wu, C. X. Wang, X. D. Fan, W. H. Zhang, X. F. Zhai, C. G. Zeng, Z. Y. Li, J. L. Yang and J. G. Hou, *Acs Nano*, 2011, **5**, 3385-3390.
36. A. Zangwill and D. D. Vvedensky, *Nano Letters*, 2011, **11**, 2092-2095.
37. B. Zhang, W. H. Lee, R. Piner, I. Kholmanov, Y. P. Wu, H. F. Li, H. X. Ji and R. S. Ruoff, *Acs Nano*, 2012, **6**, 2471-2476.
38. M. Topsakal, H. Sahin and S. Ciraci, *Physical Review B*, 2012, **85**.
39. R. Larciprete, S. Ulstrup, P. Lacovig, M. Dalmiglio, M. Bianchi, F. Mazzola, L. Hornekaer, F. Orlando, A. Baraldi, P. Hofmann and S. Lizzit, *Acs Nano*, 2012, **6**, 9551-9558.
40. S. Ulstrup, M. Andersen, M. Bianchi, L. Barreto, B. Hammer, L. Hornekaer and P. Hofmann, *2D Materials*, 2014, **1**, 025002 (025016 pp.)-025002 (025016 pp.).
41. J. C. Johannsen, S. Ulstrup, M. Bianchi, R. Hatch, D. Guan, F. Mazzola, L. Hornekaer, F. Fromm, C. Raidel, T. Seyller and P. Hofmann, *Journal of Physics-Condensed Matter*, 2013, **25**.
42. E. Granas, J. Knudsen, U. A. Schroder, T. Gerber, C. Busse, M. A. Arman, K. Schulte, J. N. Andersen and T. Michely, *Acs Nano*, 2012, **6**, 9951-9963.
43. I. Wlasny, P. Dabrowski, M. Rogala, P. J. Kowalczyk, I. Pasternak, W. Strupinski, J. M. Baranowski and Z. Klusek, *Applied Physics Letters*, 2013, **102**.
44. Y. H. Zhang, H. R. Zhang, B. Wang, Z. Y. Chen, Y. Q. Zhang, B. Wang, Y. P. Sui, B. Zhu, C. M. Tang, X. L. Li, X. M. Xie, G. H. Yu, Z. Jin and X. Y. Liu, *Applied Physics Letters*, 2014, **104**.
45. Y. P. Hsieh, M. Hofmann, K. W. Chang, J. G. Jhu, Y. Y. Li, K. Y. Chen, C. C. Yang, W. S. Chang and L. C. Chen, *Acs Nano*, 2014, **8**, 443-448.
46. Q. Zhou, S. Coh, M. L. Cohen, S. G. Louie and A. Zettl, *Physical Review B*, 2013, **88**.
47. H. B. Lyon and G. A. Somorjai, *The Journal of Chemical Physics*, 1967, **46**, 2539-2550.
48. L. Nilsson, M. Andersen, J. Bjerre, R. Balog, B. Hammer, L. Hornekaer and I. Stensgaard, *Surface Science*, 2012, **606**, 464-469.
49. E. Laegsgaard, F. Besenbacher, K. Mortensen and I. Stensgaard, *Journal of Microscopy-Oxford*, 1988, **152**, 663-669.
50. S. Ulstrup, L. Nilsson, J. A. Miwa, R. Balog, M. Bianchi, L. Hornekaer and P. Hofmann, *Physical Review B*, 2013, **88**.

51. L. G. Cancado, A. Jorio, E. H. M. Ferreira, F. Stavale, C. A. Achete, R. B. Capaz, M. V. O. Moutinho, A. Lombardo, T. S. Kulmala and A. C. Ferrari, *Nano Letters*, 2011, **11**, 3190-3196.

52. X. Yin, Y. Li, F. Ke, C. Lin, H. Zhao, L. Gan, Z. Luo, R. Zhao, T. Heinz and Z. Hu, *Nano Res.*, 2014, **7**, 1613-1622.